RESEARCH ARTICLE

MEDICAL PHYSICS

Alpha dose modeling in diffusing alpha-emitters radiation therapy—Part I: single-seed calculations in one and two dimensions

Guy Heger | **Arindam Roy** | **Mirta Dumančić** | **Lior Arazi**

Unit of Nuclear Engineering, Faculty of Engineering Sciences, Ben-Gurion University of the Negev, Be'er-Sheva, Israel

Correspondence
Lior Arazi, Unit of Nuclear Engineering, Faculty of Engineering Sciences, Ben-Gurion University of the Negev, P.O.B. 653, Be'er-Sheva 8410501, Israel.
Email: larazi@bgu.ac.il

Abstract

Background: Diffusing alpha-emitters Radiation Therapy ("DaRT") is a new method, presently in clinical trials, which allows treating solid tumors by alpha particles. DaRT relies on interstitial seeds carrying μCi-level ^{224}Ra activity below their surface, which release a chain of short-lived alpha emitters that spread throughout the tumor volume primarily by diffusion. Alpha dose calculations in DaRT are based on describing the transport of alpha emitting atoms, requiring new modeling techniques.

Purpose: A previous study introduced a simplified framework, the "Diffusion-Leakage (DL) model", for DaRT alpha dose calculations, and employed it to a point source, as a basic building block of arbitrary configurations of line sources. The aim of this work, which is divided into two parts, is to extend the model to realistic seed geometries (in Part I), and to employ single-seed calculations to study the properties of DaRT seed lattices (Part II). Such calculations can serve as a pragmatic guide for treatment planning in future clinical trials.

Methods: We derive a closed-form asymptotic solution for an infinitely long cylindrical source, and extend it to an approximate time-dependent expression that assumes a uniform temporal profile at all radial distances from the source. We then develop a finite-element one-dimensional numerical scheme for a complete time-dependent solution of this geometry and validate it against the closed-form expressions. Finally, we discuss a two-dimensional axisymmetric scheme for a complete time-dependent solution for a seed of finite diameter and length. Different solutions are compared over the relevant parameter space, providing guidelines on their usability and limitations.

Results: We show that approximating the seed as a finite line source comprised of point-like segments significantly underestimates the correct alpha dose, as predicted by the full two-dimensional calculation. The time-dependent one-dimensional solution is shown to coincide to sub-percent-level with the two-dimensional calculation in the seed midplane, and maintains an accuracy of a few percent up to ~ 2 mm from the seed edge.

Conclusions: For actual treatment plans, the full two-dimensional solution should be used to generate dose lookup tables, similarly to the TG-43 format employed in conventional brachytherapy. Given the accuracy of the one-dimensional solution up to ~ 2 mm from the seed edge it can be used for efficient parametric studies of DaRT seed lattices.

KEYWORDS
alpha dose calculations, brachytherapy, DaRT, Targeted Alpha Therapy

1 | INTRODUCTION

The radiobiology of alpha particles makes them an appealing tool for cancer treatment.[1] As a high-LET form of radiation they create irreparable clustered DNA lesions, and their cell-inactivation ability is much less affected by hypoxia or the mitotic cycle stage compared to low-LET radiation. In addition, their < 90 μm range can guarantee the sparing of surrounding healthy tissue, albeit requiring that the atoms emitting them are brought to the immediate vicinity of the cancer cells. Multiple studies are ongoing with the aim of bringing Targeted Alpha Therapy (TAT) to clinical use, with alpha emitters bound to antibodies, small molecules or nano- and micro-particles.[2–4] Presently, the only FDA-approved alpha-particle therapy involves using $^{223}RaCl_2$ to treat bone metastases in castration-resistant prostate cancer.[5]

While TAT generally focuses on single-cell or micrometastatic disease, Diffusing alpha-emitters Radiation Therapy (DaRT)[6] harnesses alpha particles for the treatment of solid tumors. In DaRT, tumors are treated with sources ("seeds") carrying a few μCi ^{224}Ra activity below their surface. Once inside the tumor, the seeds continuously release from their surface the short-lived daughter atoms of ^{224}Ra: ^{220}Rn, ^{216}Po, ^{212}Pb, ^{212}Bi, ^{212}Po and ^{208}Tl. These spread by diffusion (with possible contribution by convective effects), creating—primarily through their alpha decays—a "kill-region" measuring several millimeters in diameter around each seed. The full decay chain, along with the isotopes' half-lives, decay modes and mean alpha particle energies is shown in Figure 1.

DaRT was, and still is, extensively investigated in in vitro and in vivo preclinical studies on a large number of cancer types, as a stand-alone treatment,[6–10] in combination with chemotherapy,[11–14] and as a stimulator of a local and systemic anti-tumor immune response.[15–22] Since 2017, DaRT is under clinical investigations in human patients, starting with locally advanced and recurrent squamous cell carcinoma (SCC) of the skin and head and neck.[23] Results of the first-in-human trial were highly promising in terms of both efficacy and safety: all treated tumors shrank drastically (by $\sim$ $30\% - 100\%$), beginning in the first few days after the treatment, with $\sim$ 80% of the tumors exhibiting complete response. Adverse effects were mild to moderate, with no observable local or systemic radiation-induced damage to healthy tissue. The alpha dose to all organs, resulting from ^{212}Pb leaving the tumor through the blood, was calculated to be on the centigray level, with blood and urine activity measurements consistent with the predictions of an ICRP-based biokinetic model.[24] In one patient, untreated lesions shrank and disappeared when one lesion was treated with DaRT (in the absence
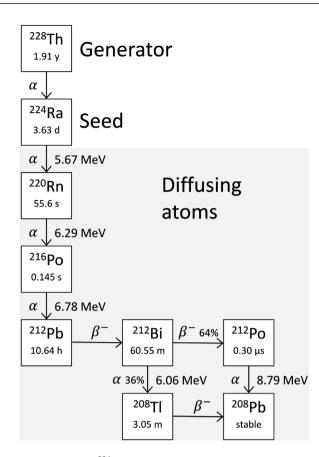

FIGURE 1 The ^{224}Ra decay chain. Data taken from the NuDat3 database website.[37]

of any other treatment), suggesting an abscopal effect.[25]

A recent publication[26] provided an in-depth description of the underlying physics of DaRT. As a first step toward treatment planning, it introduced a simplified theoretical approach: the "Diffusion-Leakage (DL) model". Its underlying assumptions are that the medium into which the daughters of ^{224}Ra are released is homogeneous, isotropic and does not change with time, and that convective effects have a short correlation length and can therefore be described by an effective isotropic diffusion term. A further assumption is that ^{212}Pb and ^{212}Bi can be cleared from the tumor through the blood at a uniform local rate. It was shown that of the six radionuclides released from the source, one only needs to model the migration of ^{220}Rn, ^{212}Pb and ^{212}Bi as their respective short-lived daughters are in local secular equilibrium. The analysis focused on the alpha particle dose of an ideal point source, which constitutes the basic building block for any arbitrary configuration of line sources.

This work forms the first part of a two-part publication, where we extend the alpha dose modeling of DaRT to cylindrical seeds of finite diameter and length. In this part the focus is on single-seed calculations,

while the second part addresses the properties of DaRT seed lattices. We derive closed-form asymptotic and approximate time-dependent solutions to the DL model for infinite cylindrical sources, and describe numerical schemes for solving the complete time-dependent problem in both one and two dimensions. We compare the 2D numerical solution to the 1D case and other approximations, and discuss the conditions under which the closed-form and 1D solutions can be used with sufficient accuracy. Detailed descriptions of an extensive experimental study on the DL model parameters in multiple tumor types, the dose contribution of beta and gamma emissions by ^{224}Ra and its daughters, and a microdosimetry analysis of cell survival and tumor control probabilities will be covered in separate publications.

2 | THE DIFFUSION-LEAKAGE MODEL IN CYLINDRICAL COORDINATES

The underlying assumptions of the DL model[26] are as follows:

- The migration of atoms inside the tumor is governed by diffusion. Convective effects have random directions and can therefore be accounted for by an effective diffusion coefficient.
- The tissue is homogeneous, isotropic, and time-independent. All coefficients appearing in the equations are therefore constant.
- It is sufficient to model the migration of ^{220}Rn, ^{212}Pb and ^{212}Bi. ^{216}Po, ^{212}Po and ^{208}Tl are in local secular equilibrium with their respective parents.
- ^{212}Pb migration can be described using a single effective diffusion coefficient.
- ^{212}Pb atoms reaching blood vessels are cleared from the tumor on a time scale that is constant throughout the tumor.
- ^{220}Rn is sufficiently short-lived to fully decay inside the tumor.
- ^{212}Bi can be cleared from the tumor similarly to ^{212}Pb (but in practice this is a second-order effect).

We consider the case of a cylindrical source of radius R_0 and length l along the z-axis, and assume axial symmetry. Under the above assumptions, in cylindrical coordinates (r, z) the equations describing the dynamics of the main daughter atoms in the decay chain— ^{220}Rn, ^{212}Pb and ^{212}Bi—are:

$$\frac{\partial n_{Rn}}{\partial t} = D_{Rn}\left(\frac{1}{r}\frac{\partial}{\partial r}\left(r\frac{\partial n_{Rn}}{\partial r}\right) + \frac{\partial^2 n_{Rn}}{\partial z^2}\right) - \lambda_{Rn}n_{Rn} \quad (1)$$

$$\frac{\partial n_{Pb}}{\partial t} = D_{Pb}\left(\frac{1}{r}\frac{\partial}{\partial r}\left(r\frac{\partial n_{Pb}}{\partial r}\right) + \frac{\partial^2 n_{Pb}}{\partial z^2}\right)$$
$$+ \lambda_{Rn}n_{Rn} - (\lambda_{Pb} + \alpha_{Pb})n_{Pb} \quad (2)$$

$$\frac{\partial n_{Bi}}{\partial t} = D_{Bi}\left(\frac{1}{r}\frac{\partial}{\partial r}\left(r\frac{\partial n_{Bi}}{\partial r}\right) + \frac{\partial^2 n_{Bi}}{\partial z^2}\right)$$
$$+ \lambda_{Pb}n_{Pb} - (\lambda_{Bi} + \alpha_{Bi})n_{Bi} \quad (3)$$

where n_{Rn}, n_{Pb}, n_{Bi}, D_{Rn}, D_{Pb}, D_{Bi} and λ_{Rn}, λ_{Pb}, λ_{Bi} are the number densities, diffusion coefficients and decay rate constants of ^{220}Rn, ^{212}Pb and ^{212}Bi, respectively. α_{Pb} and α_{Bi} are the leakage rate constants of ^{212}Pb and ^{212}Bi accounting for clearance through the blood.

The boundary conditions, for $r \rightarrow R_0$ and $|z| \leq l/2$ ($z = 0$ at the seed midplane), are:

$$2\pi R_0 j_{Rn}(R_0, z, t) = P_{des}(Rn)\frac{\Gamma_{Ra}^{src}(0)}{l}e^{-\lambda_{Ra}t} \quad (4)$$

$$2\pi R_0 j_{Pb}(R_0, z, t) = \left(P_{des}^{eff}(Pb) - P_{des}(Rn)\right)\frac{\Gamma_{Ra}^{src}(0)}{l}e^{-\lambda_{Ra}t} \quad (5)$$

$$j_{Bi}(R_0, z, t) = 0 \quad (6)$$

where $j_x = -D_x\partial n_x/\partial r$ is the radial component of the diffusion current, with x representing ^{220}Rn, ^{212}Pb and ^{212}Bi. $\Gamma_{Ra}^{src}(0)$ is the initial ^{224}Ra activity on the source (assumed to be uniform) and λ_{Ra} is the ^{224}Ra decay rate constant. $P_{des}(Rn)$ and $P_{des}^{eff}(Pb)$ are the desorption probabilities of ^{220}Rn and ^{212}Pb, respectively, representing the probability that a decay of a ^{224}Ra on the source will lead to the release of either a ^{220}Rn or ^{212}Pb atom into the tumor; we use the term "effective" for $P_{des}^{eff}(Pb)$, because it includes several emission pathways.[26] For $|z| > l/2, j_x(0, z, t) = 0$ for the three isotopes.

The solution for Equations (1)–(3) provides the number densities $n_{Rn}(r, z, t)$, $n_{Pb}(r, z, t)$ and $n_{Bi}(r, z, t)$. The alpha dose is calculated by assuming that the range of alpha particles is much smaller than the scale governing the diffusive spread, such that their energy is fully deposited at their emission point. The dose from source insertion to time t is comprised of two contributions: one is arising from the summed alpha particle energy of the pair ^{220}Rn+^{216}Po, and the other from the alpha decay of either ^{212}Bi or ^{212}Po:

$$Dose_\alpha(RnPo; r, z, t) = \frac{E_\alpha(RnPo)}{\rho}\int_0^t \lambda_{Rn}n_{Rn}(r, z, t')dt' \quad (7)$$

$$Dose_\alpha(BiPo; r, z, t) = \frac{E_\alpha(BiPo)}{\rho}\int_0^t \lambda_{Bi}n_{Bi}(r, z, t')dt' \quad (8)$$

where $E_\alpha(RnPo) = (6.288 + 6.778)$ MeV $= 13.066$ MeV is the total alpha particle energy of ^{220}Rn and ^{216}Po, $E_\alpha(BiPo) = 7.804$ MeV is the weighted-average energy of the alpha particles emitted by ^{212}Bi and ^{212}Po,

and ρ is the tissue density (assumed below to be 1.0 g/cm^3). In what follows, we define the "asymptotic dose" as the dose delivered from source insertion to infinity—in practice, over the course of several weeks.

The spread of ^{220}Rn, ^{212}Pb and ^{212}Bi is governed by their respective *diffusion lengths*,[26] defined as-

$$L_{Rn} = \sqrt{\frac{D_{Rn}}{\lambda_{Rn} - \lambda_{Ra}}} \qquad (9)$$

$$L_{Pb} = \sqrt{\frac{D_{Pb}}{\lambda_{Pb} + \alpha_{Pb} - \lambda_{Ra}}} \qquad (10)$$

$$L_{Bi} = \sqrt{\frac{D_{Bi}}{\lambda_{Bi} + \alpha_{Bi} - \lambda_{Ra}}} \qquad (11)$$

An important parameter in the DL model is the ^{212}Pb *leakage probability* $P_{leak}(Pb)$, defined as the probability that a ^{212}Pb atom released from the source is cleared from the tumor by the blood before its decay.[26] Therefore, the leakage probability reflects the competition between ^{212}Pb radioactive decay and clearance through the blood, such that:

$$P_{leak}(Pb) = \frac{\alpha_{Pb}}{\lambda_{Pb} + \alpha_{Pb}} \qquad (12)$$

The diffusion length is a gross measure of the average displacement of an atom from the location of its parent's decay, to the point of its decay or clearance by the blood. For a point source the radial dependence of the number densities and alpha dose components comprises terms proportional to $e^{-r/L_x}/r$. As discussed previously,[26] published data on the diffusion coefficients of noble gases in water and tissue[27,28] lead to an *a-priori* estimate $L_{Rn} \sim 0.2 - 0.4$ mm, where the higher limit reflects the possibility of some enhancement of effective diffusion by the tumor vascular system. For ^{212}Pb, the mass range of known lead-binding proteins, $5 - 280$ kDa,[29] corresponds to diffusion coefficients on the scale of $\sim 3 \cdot 10^{-8} - 1 \cdot 10^{-6}$ cm^2/s.[30–32] Considering the observed typical range $P_{leak}(Pb) \sim 0.2 - 0.8$ this translates to a broad *a-priori* estimate $L_{Pb} \sim 0.2 - 2$ mm. Measurements in mice-borne tumors, to be described in detail in separate publications, indicate that both 30 min and several days after seed insertion the activity pattern is governed by an effective diffusion length typically in the range of $\sim 0.2 - 0.6$ mm, depending on the tumor type and size. When analyzed in the framework of the DL model, the effective diffusion length measured 30 min after seed insertion is interpreted as L_{Rn} due to the late build-up of ^{212}Pb. The observed similar range of values of the effective diffusion length several days after seed insertion brings up the possibility that the long-term spread is also governed by ^{220}Rn, that is, that $L_{Pb} \lesssim L_{Rn}$.

In the analysis below we allow both diffusion lengths to vary across roughly similar ranges. When considering a high-diffusion scenario in tissue (where the leading diffusion parameter is greater than 0.5 mm), we take a conservative approach of $L_{Pb} > L_{Rn}$. This approach is conservative because it implies that only one alpha particle (of ^{212}Bi/^{212}Po) dominates the dose at large distances from the seed, while in the radon-dominated case the dose at large distances results from up to three alpha emissions: by ^{220}Rn, ^{216}Po and—if ^{212}Pb is not cleared by the blood—by ^{212}Bi/^{212}Po. As for the possible redistribution of ^{212}Bi relative to ^{212}Pb, measurements of the local ^{212}Bi/^{212}Pb activity ratio in SCC tumors indicate that the two isotopes are, within error, in secular equilibrium driven by ^{224}Ra,[6] which in turn implies that $\alpha_{Bi} \ll \lambda_{Bi}$ and that $L_{Bi} \lesssim 0.2 L_{Pb}$.[26] In what follows we assume $\alpha_{Bi} = 0$ and $L_{Bi} = 0.1 L_{Pb}$.

3 | ASYMPTOTIC AND APPROXIMATE TIME-DEPENDENT SOLUTIONS FOR AN INFINITELY LONG CYLINDRICAL SOURCE

At long times after source insertion into the tumor the number densities reach an asymptotic form:[26] $n_x^{asy}(r, z, t) = \tilde{n}_x(r, z)e^{-\lambda_{Ra}t}$. For ^{220}Rn this condition is satisfied within several minutes throughout the tumor, while for ^{212}Pb and ^{212}Bi the asymptotic form is attained within a few days, depending on the distance from the source.

Appendix A provides a derivation of the closed-form asymptotic solution of the DL model equations for an infinitely long cylindrical source of radius R_0. For ^{220}Rn the solution is:

$$n_{Rn}^{asy}(r, t) = A_{Rn} K_0\left(\frac{r}{L_{Rn}}\right) e^{-\lambda_{Ra}t} \qquad (13)$$

where:

$$A_{Rn} = \frac{P_{des}(Rn)\left(\Gamma_{Ra}^{src}(0)/l\right)}{2\pi D_{Rn} \cdot (R_0/L_{Rn}) \cdot K_1(R_0/L_{Rn})} \qquad (14)$$

In these expressions $K_0(\xi)$ and $K_1(\xi)$ are modified Bessel functions of the second kind:

$$K_0(\xi) = \int_0^\infty \frac{\cos(\xi t)}{\sqrt{t^2 + 1}} dt \qquad (15)$$

$$K_1(\xi) = -\frac{dK_0}{d\xi} \qquad (16)$$

$K_0(r/L)$ is a steeply-falling function, and is the cylindrical analogue to $\exp(-r/L)/(r/L)$ appearing in expressions for the number densities and dose of the point source.[26] As shown in Appendix A, for ^{212}Pb we have:

$$n_{Pb}^{asy}(r, t) = \left(A_{Pb}\, K_0\left(\frac{r}{L_{Rn}}\right) + B_{Pb}\, K_0\left(\frac{r}{L_{Pb}}\right) \right) e^{-\lambda_{Ra} t}$$

(17)

where:

$$A_{Pb} = \frac{L_{Rn}^2 L_{Pb}^2}{L_{Rn}^2 - L_{Pb}^2} \frac{\lambda_{Rn}}{D_{Pb}} A_{Rn}$$

(18)

$$B_{Pb} = \frac{\left(P_{des}^{eff}(Pb) - P_{des}(Rn) \right)\left(\Gamma_{Ra}^{src}(0)/l \right)}{2\pi D_{Pb} \cdot (R_0/L_{Pb}) \cdot K_1(R_0/L_{Pb})}$$

$$- A_{Pb} \frac{(R_0/L_{Rn}) \cdot K_1(R_0/L_{Rn})}{(R_0/L_{Pb}) \cdot K_1(R_0/L_{Pb})}$$

(19)

Finally, for ^{212}Bi the solution is:

$$n_{Bi}^{asy}(r, t) = \left(A_{Bi}\, K_0\left(\frac{r}{L_{Rn}}\right) + B_{Bi}\, K_0\left(\frac{r}{L_{Pb}}\right) \right.$$

$$\left. + C_{Bi}\, K_0\left(\frac{r}{L_{Bi}}\right) \right) e^{-\lambda_{Ra} t}$$

(20)

where:

$$A_{Bi} = \frac{L_{Rn}^2 L_{Bi}^2}{L_{Rn}^2 - L_{Bi}^2} \frac{\lambda_{Pb}}{D_{Bi}} A_{Pb}$$

(21)

$$B_{Bi} = \frac{L_{Pb}^2 L_{Bi}^2}{L_{Pb}^2 - L_{Bi}^2} \frac{\lambda_{Pb}}{D_{Bi}} B_{Pb}$$

(22)

$$C_{Bi} = -\frac{(R_0/L_{Rn}) \cdot K_1(R_0/L_{Rn}) A_{Bi} + (R_0/L_{Pb}) \cdot K_1(R_0/L_{Pb}) B_{Bi}}{(R_0/L_{Bi}) \cdot K_1(R_0/L_{Bi})}$$

(23)

As shown in Appendix A the expressions above can also describe an infinite line source in the limit $R_0/L_x \to 0$.

To approximately account for the buildup stage of the solution, one can assume that it is uniform throughout the tumor, that is, independent of the distance from the source. Under this "0D" temporal approximation[26] for a point source and adapted here for the cylindrical case, one can write:

$$n_{Rn}^{0D}(r, t) = A_{Rn}\, K_0\left(\frac{r}{L_{Rn}}\right) \left(e^{-\lambda_{Ra} t} - e^{-\lambda_{Rn} t} \right)$$

(24)

and

$$n_{Bi}^{0D}(r, t) = \left(A_{Bi}\, K_0\left(\frac{r}{L_{Rn}}\right) + B_{Bi}\, K_0\left(\frac{r}{L_{Pb}}\right) \right.$$

$$\left. + C_{Bi}\, K_0\left(\frac{r}{L_{Bi}}\right) \right) \left(e^{-\lambda_{Ra} t} - e^{-(\lambda_{Pb} + \alpha_{Pb}) t} \right)$$

(25)

Under this approximation, the asymptotic alpha dose components are:

$$Dose_\alpha^{asy}(RnPo; r) = \frac{E_\alpha(RnPo)}{\rho} \lambda_{Rn} A_{Rn}\, K_0\left(\frac{r}{L_{Rn}}\right)(\tau_{Ra} - \tau_{Rn})$$

(26)

and:

$$Dose_\alpha^{asy}(BiPo; r) = \frac{E_\alpha(BiPo)}{\rho} \lambda_{Bi}$$

$$\left(A_{Bi}\, K_0\left(\frac{r}{L_{Rn}}\right) + B_{Bi}\, K_0\left(\frac{r}{L_{Pb}}\right) + C_{Bi}\, K_0\left(\frac{r}{L_{Bi}}\right) \right)\left(\tau_{Ra} - \tau_{Pb}^{eff}\right)$$

(27)

where $\tau_{Ra} = 1/\lambda_{Ra}$, $\tau_{Rn} = 1/\lambda_{Rn}$ and $\tau_{Pb}^{eff} = 1/(\lambda_{Pb} + \alpha_{Pb})$. The error introduced by the 0D approximation is of the order of the ratio between mean lifetimes of ^{220}Rn and ^{212}Pb and that of ^{224}Ra, that is, $\tau_{Rn}/\tau_{Ra} \sim 10^{-4}$ and $\tau_{Pb}/\tau_{Ra} \sim 0.1$, respectively.

4 | FINITE-ELEMENT ONE- AND TWO-DIMENSIONAL TIME-DEPENDENT SOLUTIONS FOR CYLINDRICAL SOURCES

4.1 | Solution in one dimension

A complete time-dependent solution to the DL model can be found numerically using a finite-element approach. For the one-dimensional case, that is, infinite cylindrical or line source along the z-axis, Equations (1)–(3) are solved setting $\partial^2 n_x/\partial z^2 = 0$. The solution depends solely on the radial coordinate r. In the scheme presented here, the domain is divided into concentric cylindrical shells of equal radial width Δr. The radius of the source is R_0; Δr is chosen such that $R_0/\Delta r$ is an integer number, and Δr is considerably smaller than L_{Rn} and L_{Pb} (L_{Bi} has a negligible effect on the solution, and hence should not constrain Δr). A fully implicit scheme[33] is employed, thereby assuring the solution is stable. Starting with an initial time step Δt_0, subsequent time steps are changed adaptively according to the relative change in the solution between the current step and the previous one, requiring a maximal relative change ϵ_{tol}. A Dirichlet boundary condition of zero number densities is applied on the outer radius of the calculation domain. A detailed description of the numerical scheme is given in Appendix B.

The numerical solution was implemented in MATLAB in a code named "DART1D". As discussed in Appendix B, the solution requires the inversion of a large tridiagonal matrix, which is the most intensive part of the calculation. It was found that employing the Thomas algorithm[34] for the inversion was approximately four times faster than using MATLAB's mldivide ('\') tool,
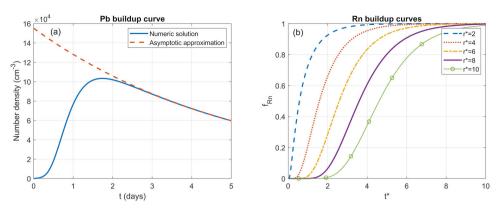
FIGURE 2 Comparison between the DART1D and asymptotic solutions for the ^{212}Pb number density 2 mm from the source (a) and the ratio between the DART1D and asymptotic solutions of the ^{220}Rn number density at various distances from the source axis (b). The distance and time are normalized to ^{220}Rn diffusion length and mean lifetime: $r^* \equiv r/L_{Rn}, t^* \equiv (\lambda_{Rn} - \lambda_{Ra})t$.
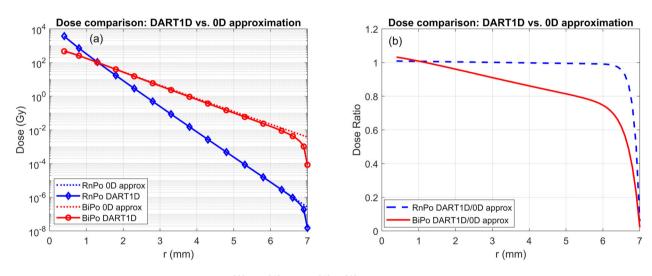

FIGURE 3 Comparison between the DART1D ^{220}Rn+^{216}Po and ^{212}Bi/^{212}Po alpha doses and the 0D approximation for an infinite cylindrical source. (a) Dose values, (b) DART1D/0D approximation ratios.

which was, in turn, about threefold faster than inverting the matrix using `inv(A)`. The code was found to converge to a sub-percent level for a modest choice of the discretization parameter values with a run time of several seconds. For example, setting $\epsilon_{tol} = 10^{-2}, \Delta r = 0.02$ mm, and $\Delta t_0 = 0.1$ s (for a domain radius $R_{max} = 7$ mm and a treatment duration of 30 d) resulted, with a runtime of ~ 0.5 s, in doses which were $\sim 0.5\%$ away from those obtained with $\epsilon_{tol} = 10^{-4}, \Delta r = 0.01$ mm and $\Delta t_0 = 0.1$ s, with a run-time of ~ 3 min (both on a modern laptop computer with an Intel i7 processor and 16 GB RAM memory). The latter, more accurate run, was within $7 \cdot 10^{-4}$ of the 0D approximation for the ^{220}Rn+^{216}Po dose.

Figures 2 and 3 examine several aspects of the numerical solution. Figure 2 shows the DART1D solution in comparison with the asymptotic expressions in Equations (13) and (17). The left panel shows the DART1D time-dependent ^{212}Pb number density at a distance of 2 mm from the source, along with the corre-

sponding asymptotic solution. On the right, we show the ratio between the numerical and asymptotic solutions for ^{220}Rn, $f_{Rn} \equiv n_{Rn}/n_{Rn}^{asy}$, plotted for varying distances from the source. The distances are given in units of the ^{220}Rn diffusion length, $r^* \equiv r/L_{Rn}$, and the time in units of $1/(\lambda_{Rn} - \lambda_{Ra})$ which is roughly the mean ^{220}Rn lifetime, $t^* \equiv (\lambda_{Rn} - \lambda_{Ra})t$. The time-dependent solutions converge to the asymptotic ones with a physical delay that increases with the distance from the source. For ^{220}Rn this occurs on the scale of minutes, while for ^{212}Pb—over a few days. The adaptive time step allows DART1D to handle both transients efficiently.

Figure 3a shows the DART1D ^{220}Rn+^{216}Po and ^{212}Bi/^{212}Po alpha dose components calculated for the case $L_{Rn} = 0.3$ mm, $L_{Pb} = 0.6$ mm, $L_{Bi} = 0.1 L_{Pb}$, $\alpha_{Pb} = \lambda_{Pb}$ (i.e., $P_{leak}(Pb) = 0.5$), and $\alpha_{Bi} = 0$. The source radius is $R_0 = 0.35$ mm, the ^{224}Ra activity is 3 μCi/cm and the desorption probabilities are $P_{des}(Rn) = 0.45$ and $P_{des}^{eff}(Pb) = 0.55$. The dose components are given

at $t = 30$ d post-treatment. The numerical calculation is compared to the 0D approximations, Equations (26) and (27). The assumption of zero number density outside the calculation domain results in a departure from the expected solution about two diffusion lengths away from the boundary: ~ 0.5 mm for ^{220}Rn and ~ 1 mm for ^{212}Bi and ^{212}Po, whose spatial distribution is governed by the ^{212}Pb diffusion length. This indicates that the radial extent of the calculation domain should be $\sim 8 - 10$ times larger than the largest diffusion length of the problem. Figure 3b shows the ratio between the DART1D-calculated dose components and the corresponding 0D approximations. Except for the edge effect at $r \to R_{max}$, the numerical solution for ^{220}Rn+^{216}Po coincides with the 0D approximation at the level of $1 \cdot 10^{-3}$ for $\epsilon_{tol} = 10^{-4}$, $\Delta r = 0.01$ mm and $\Delta t_0 = 0.1$ s up to $r \sim 5$ mm. For ^{212}Bi/^{212}Po the 0D approximation underestimates the dose at $r < 1$ mm and overestimates it at larger distances because of the increasing delay in the buildup of ^{212}Pb as a function of r. The error is $\sim 5\% - 10\%$ at therapeutically relevant distances from the source (around 2–3 mm).

4.2 | Solution in two dimensions

To accurately calculate the alpha dose for a cylindrical source of radius R_0 and length l, one needs to solve the DL model equations in two dimensions. The source lies along the z-axis with $z = 0$ at its midplane. The DL equations are solved over a cylindrical domain extending from $r = 0$ to $r = R_{max}$ and from $z = -Z_{max}$ to $z = +Z_{max}$. Both R_{max} and $Z_{max} - l/2$ should be much larger than the largest diffusion length of the problem. In the 2D scheme described here, the domain comprises ring elements of equal radial width Δr and equal z-width Δz. The values of Δr and Δz are chosen such that $R_0/\Delta r$ and $l/(2\Delta z)$ are integer numbers, with Δr and Δz much smaller than L_{Rn} and L_{Pb}. Unlike the 1D case, where the source is infinitely long and only points with $r > R_0$ are considered, for a finite seed in 2D one must also solve the equations for points above and below the seed, with $r < R_0$ and $|z| > \frac{1}{2}l$. Points inside the seed have zero number densities of ^{220}Rn, ^{212}Pb and ^{212}Bi. Similarly to the 1D case, the number densities are taken as zero on the outer boundaries of the domain. The initial time step is Δt_0, and time steps are changed adaptively to keep the relative change in the solution in consecutive steps smaller than a tolerance ϵ_{tol}.

Appendix C provides a detailed description of the 2D numerical scheme, which was implemented in MATLAB in a code named "DART2D". The code takes roughly 0.5 h to run on a modern laptop (Intel i7 processor with 16 GB RAM) for $\Delta r = 0.005$ mm, $\Delta z = 0.05$ mm, $\epsilon_{tol} = 0.01$, $\Delta t_0 = 0.1$ s, $R_{max} = 7$ mm, $Z_{max} = 10$ mm and a treatment time of 30 d. The most demanding process is matrix inversion. Since the coefficient matrix $\mathbf{M}$ is sparse and diagonal (with five non-zero diagonals), we used MATLAB's `spdiags()` function, which reduces memory requirements by saving only the diagonal non-zero elements of $\mathbf{M}$, and allows the code to run more efficiently.

The total alpha dose (sum of the ^{220}Rn+^{216}Po and ^{212}Bi/^{212}Po contributions) accumulated over 30 days of DaRT treatment by a seed of finite dimensions is displayed in the rz plane in Figure 4a. The seed dimensions are $R_0 = 0.35$ mm and $l = 10$ mm. The initial ^{224}Ra activity of the seed is 3 μCi, with $P_{des}(Rn) = 0.45$ and $P_{des}^{eff}(Pb) = 0.55$. The other model parameters are: $L_{Pb} = 0.6$ mm, $L_{Rn} = 0.3$ mm, $L_{Bi} = 0.06$ mm, $P_{leak}(Pb) = 0.5$, $\alpha_{Bi} = 0$. For presentation purpose, the calculated dose map is duplicated and mirrored around the seed axis so a symmetrical map can be shown. Consequently, negative values of r in Figure 4a refer to the mirrored values. Note that the radial dependence of the dose is nearly unchanged up to ~ 1.5 mm from the seed end. Figure 4b shows the dose profiles as a function of r in the seed midplane ($z=0$) and along z parallel to the seed axis ($r = \Delta r/2$, the ring closest to r=0), both set such that '0' is the seed edge. The dose along the seed axis is smaller by $\sim 30\%$ near the seed edge, with the difference increasing to a factor of ~ 3 at 3 mm, compared to that in the midplane—an important point to consider in treatment planning. Although a similar effect is observed when approximating the seed to a finite line source comprised of point-like segments, this approach leads to significant errors in the dose because it does not consider the finite diameter of the seed, which "pushes" the radial dose to larger values.

Figure 5 compares the results of the full 2D calculation with those obtained using three approximations: (1) an infinite cylinder with a full time-dependent calculation (using DART1D); (2) an infinite cylinder with a uniform 0D time dependence, Equations (26) and (27); and (3) a finite line source comprised of point-like segments and using the 0D approximation.[26] Panels (a) and (b) show the relative error of each approach compared to the exact 2D solution as a function of the radial distance from the source axis in its midplane. On the left we display the relative errors for a low-diffusion "radon-dominated" case, with $L_{Rn} = 0.3$ mm and $L_{Pb} = 0.1$ mm, and on the right—for a high-diffusion "lead-dominated" case, with $L_{Rn} = 0.3$ mm, $L_{Pb} = 0.6$ mm. In both cases and $P_{leak}(Pb) = 0.5$, $L_{Bi} = 0.1L_{Pb}$ and $\alpha_{Bi} = 0$. Radial distances up to 3 mm are considered because larger values are not relevant for realistic seed lattices, as discussed in Part II of this publication. Approximating the seed as a finite line source leads to underestimating the dose by $\sim 45\%$ at all distances for the low-diffusion scenario, while for the high-diffusion case underestimation starts at $\sim 40\%$ at short distances and gradually decreases with distance (where the 0D assumption
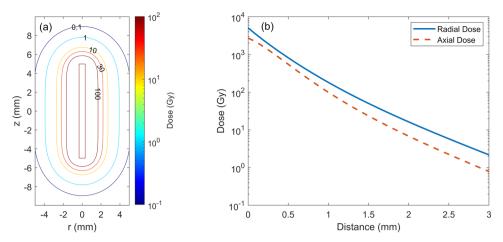
FIGURE 4 (a) Total alpha dose accumulated over 30 days of treatment by a DaRT seed with initial activity of 3μCi ^{224}Ra. The seed radius and length are 0.35 and 10 mm, respectively. The other model parameters are given in the text. Negative values of r indicate a mirrored dose map. The white space at the center represents the seed, where the number densities, and hence the dose, are zero. (b) Total alpha dose as a function of the distance from the seed edge along r in the midplane and along z on the seed axis.
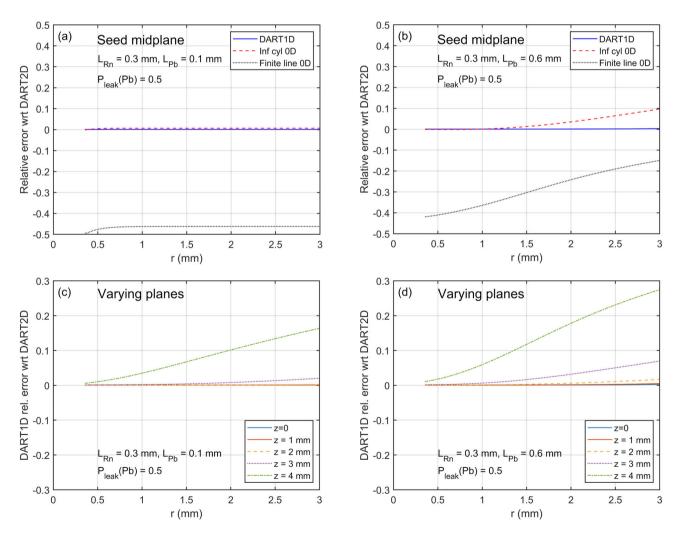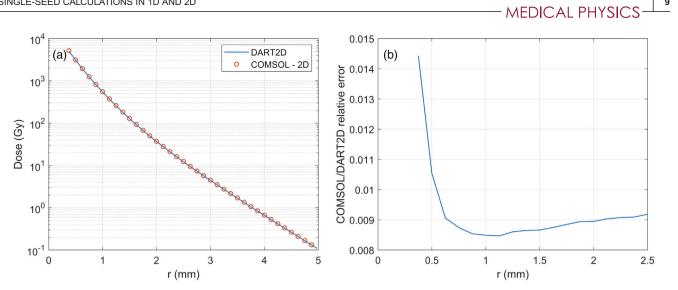

FIGURE 5 (a) and (b) Relative error in calculating the dose at the seed midplane using three approximations in comparison with the exact 2D solution (DART2D): (1) a full time-dependent solution for an infinite cylinder using DART1D; (2) closed-form solution for an infinite cylindrical source with 0D time dependence; (3) a finite line source, divided into point-like segments, with 0D time dependence. (a) Low-diffusion, radon-dominated case; (b) High-diffusion, lead-dominated case. (c) and (d) Relative error between DART1D and the dose at varying planes, as calculated by DART2D for the same choice of diffusion lengths.

FIGURE 6 (a) Total alpha particle dose calculated using DART2D and a 2D calculation in COMSOL Multiphysics[TM] for the high-diffusion "lead-dominated" case. (b) Relative error between the COMSOL Multiphysics[TM] and the DART2D calculated profiles shown in (A). The relative error is defined as $err = (COMSOL - DART2D)/DART2D$.

compensates in the opposite direction). The closed-form infinite cylinder 0D expression is accurate to $\sim 0.7\%$ at all distances for the low-diffusion case, but overestimates the dose at large distances for the high-diffusion lead-dominated case. The reason for the increased error at large distances is that the assumption of a uniform 0D time dependence does not take into account the radial variation of the delayed buildup of ^{212}Pb. This effect is seen only for the lead-dominated case, because at large distances from the source the main contribution to the dose comes from the ^{212}Bi/^{212}Po pair. Note, however, that even in this case, the relative error is below 7% up to $r \sim 2.5$ mm. The DART1D solution, with the correct time dependence, is accurate to within $\sim 0.1\% - 0.2\%$ in both scenarios. Panels (c) and (d) show the relative error in the radial dose calculated using DART1D, when compared to the correct DART2D dose at varying distances along z from the seed midplane ($z = 0$), for the low- and high-diffusion cases. DART1D is accurate within $< 5\%$ up to $z \sim 3$ mm for $r \lesssim 2.5$ mm in the high-diffusion lead-dominated case, with even better accuracy for the low-diffusion scenario.

As a final note, a comparison was done between the solutions obtained using DART2D and a 2D calculation done using COMSOL Multiphysics[TM], where the latter employed a 2D triangular mesh of varying element size and a backward differentiation formula for the adaptive time step. The goal was to check whether truncation errors resulting from the adopted 2D numerical scheme (in both space and time) have a significant effect on the solutions obtained using DART2D. The results are shown in Figure 6. The comparison shown here is for the high-diffusion "lead-dominated" case. It indicates that, although DART2D is not necessarily an optimal numerical scheme, it does lead to

$\sim 1\%$ accuracy in the therapeutically relevant region of ~ 2 mm.

5 | DISCUSSION

This work is the first part of a two-part publication on DaRT alpha dose modeling, covering single-seed dose calculations and studies of DaRT seed lattices, based on the diffusion-leakage model as a pragmatic—although clearly simplistic—framework for quantitative treatment planning in DaRT.

In this first part, we provided closed-form approximations and numerical finite-element schemes for calculating the alpha particle dose of DaRT seeds of finite diameter and length, extending the discussion of a previous publication[26] that modeled seeds as idealized line sources comprised of a collection of point-like segments. We began with the asymptotic solution of the DL model equations for infinite cylindrical sources, in analogy with the point-source case. We then employed a zero-dimensional temporal approximation to describe the initial buildup phase of both ^{220}Rn and ^{212}Pb, assuming that the time profile is independent of the radial distance from the source. For a complete time-dependent solution for infinite cylindrical sources, which properly accounts for the radial dependence of the buildup phase, we developed and described a simple one-dimensional numerical scheme ("DART1D"), and validated it against the asymptotic solutions. The extension to cylindrical sources of a finite length was done using a two-dimensional scheme ("DART2D"). We showed that the full 1D solution coincides to high accuracy with the 2D calculation in the seed midplane, and can therefore be used to validate it;

in fact, the 1D solution remains accurate to percent-level up to ~ 2 mm from the seed end. DART2D was further validated against a solution obtained with COMSOL Multiphysics^{TM}, showing that in spite of its simplicity it is accurate to $\sim 1\%$ at therapeutically relevant radial distances from the seed. A comparison between DART2D and the previous finite line-source approximation, showed that the latter considerably underestimates the accurate solution. We therefore recommend using the full 2D solution for a finite cylinder as the basis for preparing dose lookup tables for DaRT treatment planning, similarly to the TG-43 format used in conventional brachytherapy.[35]

When discussing the numerical scheme of the 1D and 2D solutions, our aim was to outline their key features rather than develop computer codes with optimized performance. The most demanding aspect of the calculation is the inversion of the coefficient matrix, which can be optimized and coded more efficiently than presented here. For example, when implemented in Fortran, DART1D completes in ~ 6 s a calculation that requires ~ 3 m to complete in MATLAB.

It is important to emphasize that while the diffusion-leakage model provides a pragmatic description of the DaRT alpha dose, it is by no means a complete theory. In particular, it does not take into account the possibility of convective effects and nonuniformity in real tumors, which comprise both necrotic and viable regions, with the former evolving as a result of the DaRT treatment itself. However, despite its limitations, the model can provide a quantitative guide for selecting a starting point for treatment planning in clinical trials in terms of seed activity and spacing. This was demonstrated in the first clinical trial,[23] where 2 μCi seeds were inserted at ~ 5 mm spacing, based on the DL model prediction that this would provide a nominal alpha dose of > 10 Gy throughout the treated volume, and where $\sim 80\%$ of the treated tumors displayed a complete response.

6 | CONCLUSION

This work brings a detailed assessment of the DL model equations and their solutions for cylindrical DaRT sources in one and two dimensions. A full numerical calculation for a DaRT seed in two dimensions is compared to a one-dimensional scheme and approximate analytical solution for an infinite cylinder. For actual treatment plans, the full two-dimensional solution should be used to generate dose lookup tables, similarly to the TG-43 format employed in conventional brachytherapy. Given the accuracy of the one-dimensional solution up to ~ 2 mm from the seed edge it can be used for efficient parametric studies of DaRT seed lattices.

CONFLICT OF INTEREST

L.A. is a minor shareholder of ATM. The scholarships of G.H. and A.R. are partially paid by ATM and that of M.D. is fully paid by ATM through a research agreement with Ben-Gurion University of the Negev. L.A. is co-inventor of several DaRT-related patents and patent applications. G.H. and M.D. are co-inventors of a pending patent application on DaRT dose calculations.

DATA AVAILABILITY STATEMENT

No experimental data was used in this article. The numerical code, along with all numerical results presented here, are available upon request to the corresponding author.

REFERENCES

1. Sgouros G, Roeske JC, McDevitt MR, et al. Committee SNM-MIRD, Bolch WE, Meredith RF, Wessels BW, Zanzonico PB. MIRD Pamphlet No. 22 (abridged): radiobiology and dosimetry of alpha-particle emitters for targeted radionuclide therapy. *J Nucl Med*. 2010;51:311–328. 20080889[pmid].
2. Targeted Alpha Therapy Working Group, Parker C, Lewington V, Shore N, et al. Targeted alpha therapy, an emerging class of cancer agents: a review. *JAMA Oncol*. 2018;4:1765–1772.
3. McDevitt MR, Sgouros G, Sofou S. Targeted and nontargeted α-particle therapies. *Annu Rev Biomed Eng*. 2018;20:73–93.
4. Guerra Liberal FD, O'Sullivan JM, McMahon SJ, Prise KM. Targeted alpha therapy: current clinical applications. *Cancer Biother Radiopharm*. 2020;35:404–417.
5. Parker C, Nilsson S, Heinrich D, et al. Alpha emitter radium-223 and survival in metastatic prostate cancer. *N Engl J Med*. 2013;369:213–223.
6. Arazi L, Cooks T, Schmidt M, Keisari Y, Kelson I. Treatment of solid tumors by interstitial release of recoiling short-lived alpha emitters. *Phys Med Biol*. 2007;52:5025–5042.
7. Cooks T, Arazi L, Schmidt M, Marshak G, Kelson I, Keisari Y. Growth retardation and destruction of experimental squamous cell carcinoma by interstitial radioactive wires releasing diffusing alpha-emitting atoms. *Int J Cancer*. 2008;122:1657–1664.
8. Cooks T, Schmidt M, Bittan H, Lazarov E, Arazi L, Kelson I, Keisari Y. Local control of lung derived tumors by diffusing alpha-emitting atoms released from intratumoral wires loaded with radium-224. *Int J Radiat Oncol Biol Physics*. 2009a;74:966–973.
9. Lazarov E, Arazi L, Efrati M, et al. Comparative in vitro microdosimetric study of murine- and human-derived cancer cells exposed to alpha particles. *Radiat Res*. 2011;177:280–287.
10. Cooks T, Tal M, Raab S, et al. Intratumoral 224Ra-loaded wires spread alpha-emitters inside solid human tumors in athymic mice achieving tumor control. *Anticancer Res*. 2012;32:5315–5321.
11. Cooks T, Arazi L, Efrati M, et al. Interstitial wires releasing diffusing alpha emitters combined with chemotherapy improved local tumor control and survival in squamous cell carcinoma-bearing mice. *Cancer*. 2009;115:1791–1801.

12. Horev-Drori G, Cooks T, Bittan H, et al. Local control of experimental malignant pancreatic tumors by treatment with a combination of chemotherapy and intratumoral 224Radium-loaded wires releasing alpha-emitting atoms. *Transl Res*. 2012;159:32–41.

13. Milrot E, Jackman A, Flescher E, et al. Enhanced killing of cervical cancer cells by combinations of methyl jasmonate with cisplatin, X or alpha radiation. *Invest New Drugs*. 2013;31:333–344.

14. Reitkopf-Brodutch S, Confino H, Schmidt M, et al. Ablation of experimental colon cancer by intratumoral 224Radium-loaded wires is mediated by alpha particles released from atoms which spread in the tumor and can be augmented by chemotherapy. *Int J Radiat Biol*. 2015;91:179–186.

15. Keisari Y, Hochman I, Confino H, Korenstein R, Kelson I. Activation of local and systemic anti-tumor immune responses by ablation of solid tumors with intratumoral electrochemical or alpha radiation treatments. *Cancer Immunol Immunother*. 2014;63:1–9.

16. Confino H, Hochman I, Efrati M, et al. Tumor ablation by intratumoral Ra-224-loaded wires induces anti-tumor immunity against experimental metastatic tumors. *Cancer Immunol Immunother*. 2015;64:191–199.

17. Confino H, Schmidt M, Efrati M, et al. Inhibition of mouse breast adenocarcinoma growth by ablation with intratumoral alpha-irradiation combined with inhibitors of immunosuppression and CpG. *Cancer Immunol Immunother*. 2016;65:1149–1158.

18. Domankevich V, Cohen A, Efrati M, et al. Combining alpha radiation-based brachytherapy with immunomodulators promotes complete tumor regression in mice via tumor-specific long-term immune response. *Cancer Immunol Immunother*. 2019;68:1949–1958.

19. Domankevich V, Efrati M, Schmidt M, et al. RIG-1-like receptor activation synergizes with intratumoral alpha radiation to induce pancreatic tumor rejection, triple-negative breast metastases clearance, and antitumor immune memory in mice. *Front Oncol*. 2020;10:990.

20. Keisari Y, Popovtzer A, Kelson I. Effective treatment of metastatic cancer by an innovative intratumoral alpha particle-mediated radiotherapy in combination with immunotherapy: a short review. *J Phys Conf Ser*. 2020;1662:012016.

21. Keisari Y, Kelson I. The potentiation of anti-tumor immunity by tumor abolition with alpha particles, protons, or carbon ion radiation and its enforcement by combination with immunoadjuvants or inhibitors of immune suppressor cells and checkpoint molecules. *Cells*. 2021;10(2):228.

22. Del Mare S, Nishri Y, Shai A, et al. Diffusing alpha-emitters radiation therapy promotes a proimmunogenic tumor microenvironment and synergizes with programmed cell death protein 1 blockade. *Int J Radiat Oncol Biol Phys*. Article in press. doi: 10.1016/j.ijrobp.2022.08.043

23. Popovtzer A, Rosenfeld E, Mizrachi A, et al. Initial safety and tumor control results from a "first-in-human" multicenter prospective trial evaluating a novel alpha-emitting radionuclide for the treatment of locally advanced recurrent squamous cell carcinomas of the skin and head and neck. *Int J Radiat Oncol Biol Phys*. 2019;106:571–578.

24. Arazi L, Cooks T, Schmidt M, Keisari Y, Kelson I. The treatment of solid tumors by alpha emitters released from 224 Ra-loaded sources–internal dosimetry analysis. *Phys Med Biol*. 2010;55:1203.

25. Bellia S, Feliciani G, Duca M, et al. Clinical evidence of abscopal effect in cutaneous squamous cell carcinoma treated with diffusing alpha emitters radiation therapy: a case report. *J Contemp Brachytherapy*. 2019;11:449–457.

26. Arazi L. Diffusing alpha-emitters radiation therapy: approximate modeling of the macroscopic alpha particle dose of a point source. *Phys Med Biol*. 2020;65:015015.

27. Jähne B, Heinz G, Dietrich W. Measurement of the diffusion coefficients of sparingly soluble gases in water. *J Geophys Res*. 1987;92:10767–10776.

28. NRC. *Risk Assessment of Radon in Drinking Water*. National Academy Press; 1999.

29. Gonick HC. Lead-binding proteins: a review. *J Toxicol*. 2011;2011:686050.

30. Jain RK. Transport of molecules in the tumor interstitium: a review. *Cancer Res*. 1987;47:3039–3051.

31. Pluen A, Boucher Y, Ramanujan S, et al. Role of tumor-host interactions in interstitial diffusion of macromolecules: Cranial vs. subcutaneous tumors. *Proc Natl Acad Sci*. 2001;98:4628–4633.

32. Brown EB, Boucher Y, Nasser S, Jain RK. Measurement of macromolecular diffusion coefficients in human tumors. *Microvasc Res*. 2004;67:231–236.

33. Press WH, Teukolsky SA, Vetterling WT, Flannery BP. *Numerical Recipes 3rd Edition: The Art of Scientific Computing*. Cambridge University Press; 2007.

34. Kis T. Tridiagonal Matrix Algorithm (Thomas Alg.) (tridiagonal), 2021. Accessed: September 28, 2021.

35. Rivard MJ, Coursey BM, DeWerd LA, et al. Update of AAPM Task Group No. 43 Report: a revised AAPM protocol for brachytherapy dose calculations. *Med Phys*. 2004;31:633–674.

36. Abramowitz M, Stegun IA, eds., *Handbook of Mathematical Functions with Formulas, Graphs, and Mathematical Tables, 9th printing*, chapter "Modified Bessel Functions I and K" section 9.6, pp. 374–377. Dover; 1972.

37. Nudat3 database, National Nuclear Data Center.

APPENDIX A: DERIVATION OF THE ASYMPTOTIC SOLUTIONS FOR INFINITE CYLINDRICAL AND LINE SOURCES

In this appendix we provide a detailed derivation of the asymptotic solutions of the diffusion-leakage model equations for the number densities of ^{220}Rn, ^{212}Pb and ^{212}Bi, for an infinite cylindrical source and infinite line source.

A.1 | ^{220}Rn

The ^{220}Rn diffusion equation for the case of an infinite cylindrical source of radius R_0 in a homogeneous and isotropic medium, in cylindrical coordinates, is:

$$\frac{\partial n_{Rn}}{\partial t} = \frac{D_{Rn}}{r}\frac{\partial}{\partial r}\left(r\frac{\partial n_{Rn}}{\partial r}\right) + s_{Rn} - \lambda_{Rn}n_{Rn} \quad (A1)$$

Assuming no ^{224}Ra release from the source $s_{Rn}(r, t) = 0$, and ^{220}Rn enters the tumor by direct release from the source surface, with the following boundary condition at

$r \rightarrow R_0$:

$$\lim_{r \rightarrow R_0} 2\pi r j_{Rn}(r, t) = P_{des}(Rn)\frac{\Gamma_{Ra}^{src}(0)}{l}e^{-\lambda_{Ra}t} \quad (A2)$$

where $\Gamma_{Ra}^{src}(0)/l$ is the initial ^{224}Ra activity per unit length of the source, and $j_{Rn} = -D_{Rn}\frac{\partial n_{Rn}}{\partial r}$. Substituting the asymptotic form $n_{Rn}^{asy}(r, t) = \widetilde{n}_{Rn}(r)e^{-\lambda_{Ra}t}$ in Equation (A1) leads to:

$$\frac{d^2\widetilde{n}_{Rn}}{dr^2} + \frac{1}{r}\frac{d\widetilde{n}_{Rn}}{dr} - \frac{1}{L_{Rn}^2}\widetilde{n}_{Rn} = 0 \quad (A3)$$

where L_{Rn} is defined in Equation (9). Defining $\xi = r/L_{Rn}$ gives:

$$\xi^2\frac{d^2\widetilde{n}_{Rn}}{d\xi^2} + \xi\frac{d\widetilde{n}_{Rn}}{d\xi} - (\xi^2 + n^2)\widetilde{n}_{Rn} = 0 \quad (A4)$$

with $n = 0$. This has the form of a modified Bessel equation,[36] for which the solution is:

$$\widetilde{n}_{Rn}(\xi) = A_{Rn}K_0(\xi) + B_{Rn}I_0(\xi) \quad (A5)$$

$I_0(\xi)$ is a modified Bessel function of the first kind. Since it diverges for $\xi \rightarrow \infty$, it must hold that $B_{Rn} = 0$. $K_0(\xi)$ is a modified Bessel function of the second kind, for which:

$$K_0(\xi) = \int_0^\infty \frac{\cos(\xi t)}{\sqrt{t^2 + 1}}dt \quad (A6)$$

It vanishes in the limit $\xi \rightarrow \infty$ and hence:

$$\widetilde{n}_{Rn}(\xi) = A_{Rn}K_0(\xi) \quad (A7)$$

The modified Bessel functions of the second kind have the property that:

$$\xi\frac{dK_n}{d\xi} = nK_n(\xi) - \xi K_{n+1}(\xi) \quad (A8)$$

Thus:

$$\frac{dK_0}{d\xi} = -K_1(\xi) \quad (A9)$$

Using this, the current can be expressed as:

$$j_{Rn}(r, t) = \frac{D_{Rn}}{L_{Rn}}A_{Rn}K_1\left(\frac{r}{L_{Rn}}\right)e^{-\lambda_{Ra}t} \quad (A10)$$

Substituting (A10) into the boundary condition (A2) yields:

$$A_{Rn} = \frac{P_{des}(Rn)\left(\Gamma_{Ra}^{src}(0)/l\right)}{2\pi D_{Rn}(R_0/L_{Rn})K_1(R_0/L_{Rn})} \quad (A11)$$

Finally:

$$n_{Rn}^{asy}(r, t) = \frac{P_{des}(Rn)\left(\Gamma_{Ra}^{src}(0)/l\right)}{2\pi D_{Rn}(R_0/L_{Rn})K_1(R_0/L_{Rn})}K_0\left(\frac{r}{L_{Rn}}\right)e^{-\lambda_{Ra}t} \quad (A12)$$

For $\xi \rightarrow 0$:[36]

$$\lim_{\xi \rightarrow 0} \xi K_1(\xi) = 1 \quad (A13)$$

Therefore, for the case of an ideal line source $(R_0/L_{Rn} \rightarrow 0)$:

$$n_{Rn}^{asy}(r, t) = \frac{P_{des}(Rn)\left(\Gamma_{Ra}^{src}(0)/l\right)}{2\pi D_{Rn}}K_0\left(\frac{r}{L_{Rn}}\right)e^{-\lambda_{Ra}t} \quad (A14)$$

A.2 | ^{212}Pb

The diffusion-leakage equation for ^{212}Pb for the infinite cylindrical source geometry is:

$$\frac{\partial n_{Pb}}{\partial t} = \frac{D_{Pb}}{r}\frac{\partial}{\partial r}\left(r\frac{\partial n_{Pb}}{\partial r}\right) - \lambda_{Pb}n_{Pb} - \alpha_{Pb}n_{Pb} + \lambda_{Rn}n_{Rn} \quad (A15)$$

with the boundary condition:

$$\lim_{r \rightarrow R_0} 2\pi r j_{Pb}(r, t) = \left(P_{des}^{eff}(Pb) - P_{des}(Rn)\right)\frac{\Gamma_{Ra}^{src}(0)}{l}e^{-\lambda_{Ra}t} \quad (A16)$$

where $j_{Pb} = -D_{Pb}\frac{\partial n_{Pb}}{\partial r}$. As before, the solution is assumed to take the form:

$$n_{Pb}^{asy}(r, t) = \widetilde{n}_{Pb}(r)e^{-\lambda_{Ra}t} \quad (A17)$$

Substituting the asymptotic forms for ^{212}Pb and ^{220}Rn in Equation (A15) yields:

$$(\lambda_{Pb} + \alpha_{Pb} - \lambda_{Ra})\widetilde{n}_{Pb} = D_{Pb}\left(\frac{d^2\widetilde{n}_{Pb}}{dr^2} + \frac{1}{r}\frac{d\widetilde{n}_{Pb}}{dr}\right)$$
$$+ \lambda_{Rn}A_{Rn}K_0\left(\frac{r}{L_{Rn}}\right) \quad (A18)$$

where A_{Rn} is given in (A11). Using the definition of L_{Pb} (10), this can be written as:

$$\left(\frac{d^2\tilde{n}_{Pb}}{dr^2} + \frac{1}{r}\frac{d\tilde{n}_{Pb}}{dr}\right) - \frac{1}{L_{Pb}^2}\tilde{n}_{Pb} + \frac{\lambda_{Rn}}{D_{Pb}}A_{Rn}K_0\left(\frac{r}{L_{Rn}}\right) = 0 \quad \text{(A19)}$$

We attempt a solution of the form:

$$\tilde{n}_{Pb}(r) = A_{Pb}K_0\left(\frac{r}{L_{Rn}}\right) + B_{Pb}K_0\left(\frac{r}{L_{Pb}}\right) \quad \text{(A20)}$$

In order to proceed, some properties of the modified Bessel functions need to be utilised. Again, we define $\xi = r/L$. Using the recursion relation (A8), we have:

$$\frac{dK_0}{d\xi} = -K_1(\xi) \quad \text{(A21)}$$

$$\frac{dK_1}{d\xi} = \frac{1}{\xi}K_1(\xi) - K_2(\xi) \quad \text{(A22)}$$

Another property of the modified Bessel functions[36] is:

$$K_{n+1}(\xi) = K_{n-1}(\xi) + \frac{2n}{\xi}K_n(\xi) \quad \text{(A23)}$$

Thus:

$$K_2(\xi) = K_0(\xi) + \frac{2}{\xi}K_1(\xi) \quad \text{(A24)}$$

Substituting $K_2(\xi)$ from (A24) in (A22) gives:

$$\frac{dK_1}{d\xi} = -\left(K_0(\xi) + \frac{1}{\xi}K_1(\xi)\right) \quad \text{(A25)}$$

From (A21):

$$\frac{d}{dr}K_0\left(\frac{r}{L}\right) = \frac{1}{L}\frac{d}{d\xi}K_0(\xi) = -\frac{1}{L}K_1\left(\frac{r}{L}\right) \quad \text{(A26)}$$

and from (A25):

$$\frac{d}{dr}K_1\left(\frac{r}{L}\right) = \frac{1}{L}\frac{d}{d\xi}K_1(\xi) = -\frac{1}{L}\left(K_0\left(\frac{r}{L}\right) + \frac{L}{r}K_1\left(\frac{r}{L}\right)\right) \quad \text{(A27)}$$

Using results (A26) and (A27), we get:

$$\frac{d\tilde{n}_{Pb}}{dr} = -\frac{A_{Pb}}{L_{Rn}}K_1\left(\frac{r}{L_{Rn}}\right) - \frac{B_{Pb}}{L_{Pb}}K_1\left(\frac{r}{L_{Pb}}\right) \quad \text{(A28)}$$

and:

$$\frac{d^2\tilde{n}_{Pb}}{dr^2} = \frac{A_{Pb}}{L_{Rn}^2}\left(K_0\left(\frac{r}{L_{Rn}}\right) + \frac{L_{Rn}}{r}K_1\left(\frac{r}{L_{Rn}}\right)\right)$$

$$+ \frac{B_{Pb}}{L_{Pb}^2}\left(K_0\left(\frac{r}{L_{Pb}}\right) + \frac{L_{Pb}}{r}K_1\left(\frac{r}{L_{Pb}}\right)\right) \quad \text{(A29)}$$

resulting in:

$$\frac{d^2\tilde{n}_{Pb}}{dr^2} + \frac{1}{r}\frac{d\tilde{n}_{Pb}}{dr} = \frac{A_{Pb}}{L_{Rn}^2}K_0\left(\frac{r}{L_{Rn}}\right) + \frac{B_{Pb}}{L_{Pb}^2}K_0\left(\frac{r}{L_{Pb}}\right) \quad \text{(A30)}$$

When (A30) is inserted in Equation (A19), the $K_0(r/L_{Pb})$ terms cancel out, leaving:

$$A_{Pb} = \frac{L_{Rn}^2 L_{Pb}^2}{L_{Rn}^2 - L_{Pb}^2}\frac{\lambda_{Rn}}{D_{Pb}}A_{Rn}$$

$$= \frac{L_{Rn}^2 L_{Pb}^2}{L_{Rn}^2 - L_{Pb}^2}\frac{\lambda_{Rn}}{D_{Pb}}\frac{P_{des}(Rn)\left(\Gamma_{Ra}^{src}(0)/l\right)}{2\pi D_{Rn}(R_0/L_{Rn})K_1(R_0/L_{Rn})} \quad \text{(A31)}$$

The coefficient B_{Pb} is found from the boundary condition (A16). Defining $\tilde{j}_{Pb}(r) = -D_{Pb}\frac{d\tilde{n}_{Pb}}{dr}$ and using (A28), we have:

$$2\pi R_0\tilde{j}_{Pb}(R_0) = 2\pi R_0 D_{Pb}\left(\frac{A_{Pb}}{L_{Rn}}K_1\left(\frac{R_0}{L_{Rn}}\right) + \frac{B_{Pb}}{L_{Pb}}K_1\left(\frac{R_0}{L_{Pb}}\right)\right)$$

$$= \left(P_{des}^{eff}(Pb) - P_{des}(Rn)\right)\frac{\Gamma_{Ra}^{src}(0)}{l} \quad \text{(A32)}$$

yielding:

$$B_{Pb} = \frac{\left(P_{des}^{eff}(Pb) - P_{des}(Rn)\right)\left(\Gamma_{Ra}^{src}(0)/l\right)}{2\pi D_{Pb}(R_0/L_{Pb})K_1(R_0/L_{Pb})}$$

$$- A_{Pb}\frac{(R_0/L_{Rn})K_1(R_0/L_{Rn})}{(R_0/L_{Pb})K_1(R_0/L_{Pb})} \quad \text{(A33)}$$

For an ideal line source, $(R_0/L)K_1(R_0/L) \to 1$ giving:

$$A_{Pb}^{line} = \frac{L_{Rn}^2 L_{Pb}^2}{L_{Rn}^2 - L_{Pb}^2}\frac{\lambda_{Rn}}{D_{Pb}}\frac{P_{des}(Rn)\left(\Gamma_{Ra}^{src}(0)/l\right)}{2\pi D_{Rn}} \quad \text{(A34)}$$

$$B_{Pb}^{line} = \frac{\left(P_{des}^{eff}(Pb) - P_{des}(Rn)\right)\left(\Gamma_{Ra}^{src}(0)/I\right)}{2\pi D_{Pb}} - A_{Pb}$$

(A35)

Finally, we have:

$$n_{Pb}^{asy}(r, t) = \left(A_{Pb}K_0\left(\frac{r}{L_{Rn}}\right) + B_{Pb}K_0\left(\frac{r}{L_{Pb}}\right)\right)e^{-\lambda_{Ra}t}$$

(A36)

A.3 | ^{212}Bi

The diffusion-leakage equation for ^{212}Bi for an infinite cylindrical source is:

$$\frac{\partial n_{Bi}}{\partial t} = \frac{D_{Bi}}{r}\frac{\partial}{\partial r}\left(r\frac{\partial n_{Bi}}{\partial r}\right) - \lambda_{Bi}n_{Bi} - \alpha_{Bi}n_{Bi} + \lambda_{Pb}n_{Pb}$$

(A37)

Since ^{212}Bi atoms are not emitted directly from the source, the boundary condition is:

$$\lim_{r \to R_0} 2\pi r j_{Bi}(r, t) = 0$$

(A38)

We look for an asymptotic solution of the form: $n_{Bi}^{asy}(r, t) = \tilde{n}_{Bi}(r)e^{-\lambda_{Ra}t}$, attempting:

$$\tilde{n}_{Bi}(r) = A_{Bi}K_0\left(\frac{r}{L_{Rn}}\right) + B_{Bi}K_0\left(\frac{r}{L_{Pb}}\right) + C_{Bi}K_0\left(\frac{r}{L_{Bi}}\right)$$

(A39)

Substituting the asymptotic form (A39) in Equation (A37) and in the boundary condition (A38), using the asymptotic form of the ^{212}Pb solution (A36) and the expression for the effective ^{212}Bi diffusion length (11), gives:

$$n_{Bi}^{asy}(r, t) = \left(A_{Bi}K_0\left(\frac{r}{L_{Rn}}\right) + B_{Bi}K_0\left(\frac{r}{L_{Pb}}\right)\right.$$
$$\left. + C_{Bi}K_0\left(\frac{r}{L_{Bi}}\right)\right)e^{-\lambda_{Ra}t}$$

(A40)

For a cylindrical source of radius R_0:

$$A_{Bi} = \frac{L_{Rn}^2 L_{Bi}^2}{L_{Rn}^2 - L_{Bi}^2}\frac{\lambda_{Pb}}{D_{Bi}}A_{Pb}$$

(A41)

$$B_{Bi} = \frac{L_{Pb}^2 L_{Bi}^2}{L_{Pb}^2 - L_{Bi}^2}\frac{\lambda_{Pb}}{D_{Bi}}B_{Pb}$$

(A42)

$$C_{Bi} = -\frac{(R_0/L_{Rn})K_1(R_0/L_{Rn})A_{Bi} + (R_0/L_{Pb})K_1(R_0/L_{Pb})B_{Bi}}{(R_0/L_{Bi})K_1(R_0/L_{Bi})}$$

(A43)

where A_{Pb} and B_{Pb} are given in (A31) and (A33). For an infinite line source, A_{Pb} and B_{Pb} are replaced by their line source forms (A34) and (A35) and:

$$C_{Bi}^{line} = -(A_{Bi} + B_{Bi})$$

(A44)

APPENDIX B: DART1D: NUMERICAL SCHEME

In this section we provide a detailed description of the one-dimensional numerical scheme ("DART1D") used to solve the DL model equation for an infinitely long cylindrical source.

As noted in Section 4.1, the domain is divided into concentric cylindrical shells, enumerated $i = 1 \ldots N_r$, of equal radial width Δr. The radius of the source is R_0; Δr is chosen such that $R_0/\Delta r$ is an integer number, and Δr is considerably smaller than L_{Rn} and L_{Pb}. The central radius of the i-th shell is:

$$r_i = R_0 + (i - \frac{1}{2})\Delta r$$

(B1)

The average number densities in the i-th shell are $n_{Rn,i}$, $n_{Pb,i}$ and $n_{Bi,i}$. The time steps are enumerated by p. For shells away from the source surface, with $1 < i \leq N_r$, the diffusive term appearing in Equation A1, A15 and A37 is discretized as follows:

$$\frac{D_x}{r}\frac{\partial}{\partial r}\left(r\frac{\partial n_x}{\partial r}\right)_{r_i} \Longrightarrow \frac{D_x}{r_i}\frac{\left(r\frac{\partial n_x}{\partial r}\right)_{r_i+\Delta r/2} - \left(r\frac{\partial n_x}{\partial r}\right)_{r_i-\Delta r/2}}{\Delta r}$$

$$\Longrightarrow \frac{D_x}{r_i}\frac{(r_i + \frac{\Delta r}{2})\frac{n_{x,i+1}-n_{x,i}}{\Delta r} - (r_i - \frac{\Delta r}{2})\frac{n_{x,i}-n_{x,i-1}}{\Delta r}}{\Delta r}$$

$$= \frac{D_x}{\Delta r^2}\left(\left(1 + \frac{\Delta r}{2r_i}\right)n_{x,i+1} + \left(1 - \frac{\Delta r}{2r_i}\right)n_{x,i-1} - 2n_{x,i}\right)$$

(B2)

where x stands for Rn, Pb and Bi. The relative truncation error introduced by this discretization scheme in the diffusive term can be estimated from the closed-form expressions for the asymptotic number densities of the diffusing atoms. For example, for ^{220}Rn (Equation A14) it is of the order of $(\Delta r/L_{Rn})^2$.

Using Equation B2, for shells with $1 < i \leq N_r$, the DL model equations take the discrete implicit form:

$$\frac{n_{x,i}^{(p+1)} - n_{x,i}^{(p)}}{\Delta t}$$

$$= D_x\left(\frac{n_{x,i+1}^{(p+1)} + n_{x,i-1}^{(p+1)} - 2n_{x,i}^{(p+1)}}{\Delta r^2} + \frac{1}{r_i}\frac{n_{x,i+1}^{(p+1)} - n_{x,i-1}^{(p+1)}}{2\Delta r}\right)$$

$$- (\lambda_x + \alpha_x)n_{x,i}^{(p+1)} + s_{x,i}^{(p+1)}$$

(B3)

with $\alpha_{Rn} = 0$. Outside our domain the number densities are set to zero, such that in Equation (B3) for $i = N_r$ $n_{x,i+1} = 0$.

In the special case $i = 1$, i.e., the shell immediately outside the source surface with $r_1 = R_0 + \Delta r/2$, we use the boundary conditions at $r \to R_0$. Since the current density is $j_x = -D_x \frac{\partial n_x}{\partial r}$, one can write:

$$\frac{D_x}{r}\frac{\partial}{\partial r}\left(r\frac{\partial n_x}{\partial r}\right)_{r_1}$$

$$\implies \frac{D_x}{R_0 + \Delta r/2}\frac{(R_0+\Delta r)\left(\frac{\partial n_x}{\partial r}\right)_{R_0+\Delta r} - R_0\left(\frac{\partial n_x}{\partial r}\right)_{R_0}}{\Delta r}$$

$$\implies \frac{D_x}{R_0 + \Delta r/2}\frac{(R_0+\Delta r)\frac{n_{x,2}-n_{x,1}}{\Delta r} + R_0\frac{j_x(R_0,t)}{D_x}}{\Delta r} \quad (B4)$$

The source boundary conditions Equation (4)-(6) give:

$$R_0 j_{Rn}(R_0, t) = \frac{1}{2\pi}P_{des}(Rn)\frac{\Gamma_{Ra}^{src}(0)}{I}e^{-\lambda_{Ra}t} \quad (B5)$$

$$R_0 j_{Pb}(R_0, t) = \frac{1}{2\pi}\left(P_{des}^{eff}(Pb) - P_{des}(Rn)\right)\frac{\Gamma_{Ra}^{src}(0)}{I}e^{-\lambda_{Ra}t} \quad (B6)$$

$$R_0 j_{Bi}(R_0, t) = 0 \quad (B7)$$

Therefore:

$$\frac{D_{Rn}}{r}\frac{\partial}{\partial r}\left(r\frac{\partial n_{Rn}}{\partial r}\right)_{r_1}$$

$$\implies \frac{D_{Rn}}{\Delta r^2}\left(\frac{1 + \Delta r/R_0}{1 + \Delta r/2R_0}\right)(n_{Rn,2} - n_{Rn,1})$$

$$+ \frac{P_{des}(Rn)\left(\Gamma_{Ra}^{src}(0)/I\right)e^{-\lambda_{Ra}t}}{2\pi R_0 \Delta r(1 + \Delta r/2R_0)} \quad (B8)$$

$$\frac{D_{Pb}}{r}\frac{\partial}{\partial r}\left(r\frac{\partial n_{Pb}}{\partial r}\right)_{r_1} \implies \frac{D_{Pb}}{\Delta r^2}\left(\frac{1 + \Delta r/R_0}{1 + \Delta r/2R_0}\right)(n_{Pb,2} - n_{Pb,1})$$

$$+ \frac{\left(P_{des}^{eff}(Pb) - P_{des}(Rn)\right)\left(\Gamma_{Ra}^{src}(0)/I\right)e^{-\lambda_{Ra}t}}{2\pi R_0 \Delta r(1 + \Delta r/2R_0)} \quad (B9)$$

and

$$\frac{D_{Bi}}{r}\frac{\partial}{\partial r}\left(r\frac{\partial n_{Bi}}{\partial r}\right)_{r_1} \implies \frac{D_{Bi}}{\Delta r^2}\left(\frac{1 + \Delta r/R_0}{1 + \Delta r/2R_0}\right)(n_{Bi,2} - n_{Bi,1})$$

$$(B10)$$

With these expressions for the diffusive term, for the $i = 1$ shell Equation B3 becomes:

$$\frac{n_{x,1}^{(p+1)} - n_{x,1}^{(p)}}{\Delta t} = \frac{D_x}{\Delta r^2}\left(\frac{1 + \Delta r/R_0}{1 + \Delta r/2R_0}\right)\left(n_{x,2}^{(p+1)} - n_{x,1}^{(p+1)}\right)$$

$$- (\lambda_x + \alpha_x)n_{x,1}^{(p+1)} + s_{x,1}^{(p+1)} \quad (B11)$$

The source terms $s_{x,i}^{p+1}$ appearing in Equation (B3) and (B10) are:

$$s_{Rn,i}^{p+1} = \frac{P_{des}(Rn)\left(\Gamma_{Ra}^{src}(0)/I\right)e^{-\lambda_{Ra}t_{p+1}}}{2\pi R_0 \Delta r(1 + \Delta r/2R_0)}\delta_{i,1} \quad (B12)$$

$$s_{Pb,i}^{p+1} = \frac{\left(P_{des}^{eff}(Pb) - P_{des}(Rn)\right)\left(\Gamma_{Ra}^{src}(0)/I\right)e^{-\lambda_{Ra}t_{p+1}}}{2\pi R_0 \Delta r(1 + \Delta r/2R_0)}\delta_{i,1} + \lambda_{Rn}n_{Rn,i}^{p+1}$$

$$(B13)$$

$$s_{Bi,i}^{p+1} = \lambda_{Pb}n_{Pb,i}^{p+1} \quad (B14)$$

where $\delta_{i,1} = 1$ for $i = 1$ and zero otherwise. Rearranging Equation (B3) and (B10), we obtain the general form:

$$n_{x,i}^{(p)} + s_{x,i}^{(p+1)}\Delta t = A_{i,i-1}^{(x)}n_{x,i-1}^{(p+1)} + A_{i,i}^{(x)}n_{x,i}^{(p+1)} + A_{i,i+1}^{(x)}n_{x,i+1}^{(p+1)}$$

$$(B15)$$

The matrix coefficients introduced in Equation (B14) depend on the value of i, reflecting the boundary conditions for $i = 1$ and $i = N_r$. Retaining terms up to first order in $\Delta r/r_i$ the different cases are summarized below:

$$A_{i,i-1}^{(x)} = -\frac{D_x\Delta t}{\Delta r^2}\left(1 - \frac{\Delta r}{2r_i}\right) \qquad 1 < i \leq N_r$$

$$A_{i,i}^{(x)} = 1 + \frac{D_x\Delta t}{\Delta r^2}\left(1 + \frac{\Delta r}{2r_i}\right) + (\lambda_x + \alpha_x)\Delta t \qquad i = 1$$

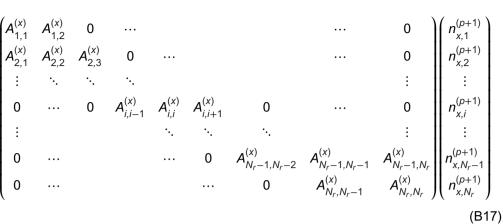$$= 1 + \frac{2D_x\Delta t}{\Delta r^2} + (\lambda_x + \alpha_x)\Delta t \qquad 1 < i \leq N_r$$

$$A_{i,i+1}^{(x)} = -\frac{D_x\Delta t}{\Delta r^2}\left(1 + \frac{\Delta r}{2r_i}\right) \qquad 1 \leq i < N_r$$

$$(B16)$$

with r_i given in Equation (B1). Writing Equation (B14) in matrix form:

(e.g., at 2 mm):

$$
\begin{pmatrix} n_{x,1}^{(p)} \\ n_{x,2}^{(p)} \\ \vdots \\ n_{x,i}^{(p)} \\ \vdots \\ n_{x,N_r-1}^{(p)} \\ n_{x,N_r}^{(p)} \end{pmatrix} + \begin{pmatrix} s_{x,1}^{(p+1)} \\ s_{x,2}^{(p+1)} \\ \vdots \\ s_{x,i}^{(p+1)} \\ \vdots \\ s_{x,N_r-1}^{(p+1)} \\ s_{x,N_r}^{(p+1)} \end{pmatrix} \Delta t_{p+1} = \begin{pmatrix} A_{1,1}^{(x)} & A_{1,2}^{(x)} & 0 & \cdots & & \cdots & 0 \\ A_{2,1}^{(x)} & A_{2,2}^{(x)} & A_{2,3}^{(x)} & 0 & \cdots & & \cdots & 0 \\ \vdots & \ddots & \ddots & \ddots & & & & \vdots \\ 0 & \cdots & 0 & A_{i,i-1}^{(x)} & A_{i,i}^{(x)} & A_{i,i+1}^{(x)} & 0 & \cdots & 0 \\ \vdots & & & & \ddots & \ddots & \ddots & & \vdots \\ 0 & \cdots & & & \cdots & 0 & A_{N_r-1,N_r-2}^{(x)} & A_{N_r-1,N_r-1}^{(x)} & A_{N_r-1,N_r}^{(x)} \\ 0 & \cdots & & & & \cdots & 0 & A_{N_r,N_r-1}^{(x)} & A_{N_r,N_r}^{(x)} \end{pmatrix} \begin{pmatrix} n_{x,1}^{(p+1)} \\ n_{x,2}^{(p+1)} \\ \vdots \\ n_{x,i}^{(p+1)} \\ \vdots \\ n_{x,N_r-1}^{(p+1)} \\ n_{x,N_r}^{(p+1)} \end{pmatrix}
$$

(B17)

which can be written as $\mathbf{n}_x^{(p)} + \mathbf{s}_x^{(p+1)}\Delta t = \mathbf{A}_x \mathbf{n}_x^{(p+1)}$. Multiplying on the left by the inverse of $\mathbf{A}_x$ gives:

$$
\mathbf{n}_x^{(p+1)} = \mathbf{A}_x^{-1}(\mathbf{n}_x^{(p)} + \mathbf{s}_x^{(p+1)}\Delta t), \tag{B18}
$$

which completes the solution for the $p + 1$ step. Note that although the source terms are calculated for the $p + 1$ step they are, in fact, known when the matrix equations are solved. The reason is that in the $p + 1$ step one first solves for ^{220}Rn, then for ^{212}Pb and lastly for ^{212}Bi. The source term for ^{220}Rn depends only on time, those of ^{212}Pb are found using the $p + 1$ solution for ^{220}Rn, and those of ^{212}Bi – using the $p + 1$ solution for ^{212}Pb. Another point to consider is that since Δt is changed consecutively in the calculation and the matrix coefficients depend on Δt, they must be updated accordingly in each step.

The alpha dose components are also updated in each step:

$$
Dose_\alpha^{(p+1)}(RnPo; i) = Dose_\alpha^{(p)}(RnPo; i) + \frac{E_\alpha(RnPo)}{\rho}\lambda_{Rn} n_{Rn,i}^{(p+1)}\Delta t \tag{B19}
$$

$$
Dose_\alpha^{(p+1)}(BiPo; i) = Dose_\alpha^{(p)}(BiPo; i) + \frac{E_\alpha(BiPo)}{\rho}\lambda_{Bi} n_{Bi,i}^{(p+1)}\Delta t \tag{B20}
$$

At the end of the $p + 1$ step, Δt is updated based on the relative change in the solution. This can be done in a number of ways. A particular choice, implemented here, was to consider the relative change in the total dose (sum of the *RnPo* and *BiPo* contributions) at a particular point of interest r_{i_0}

$$
\Delta t_{new} = \Delta t \cdot \frac{\epsilon_{tol}}{\left(Dose_\alpha^{(p+1)}(tot; i_0) - Dose_\alpha^{(p)}(tot; i_0)\right)/Dose_\alpha^{(p)}(tot; i_0)} \tag{B21}
$$

where ϵ_{tol} is a preset tolerance parameter. For practicality, one can further set upper and lower limits on Δt to balance between calculation time and accuracy. Although the initial time step should be small compared to ^{220}Rn half-life, its particular value has little effect on the accuracy of the calculated asymptotic dose.

APPENDIX C: DART2D: NUMERICAL SCHEME

In this section we provide a detailed description of the two-dimensional axisymmetric numerical scheme ("DART2D") used to solve the DL model equation for a cylindrical source of radius R_0 and length l.

The source lies along the z-axis with $z = 0$ at its midplane. The DL equations are solved over a cylindrical domain extending from $r = 0$ to $r = R_{max}$ and from $z = -Z_{max}$ to $z = +Z_{max}$. Both R_{max} and $Z_{max} - l/2$ should be much larger than the largest diffusion length of the problem. The domain comprises ring elements of equal radial width Δr and equal z-width Δz. Δr and Δz are chosen such that $R_0/\Delta r$ and $l/(2\Delta z)$ are integer numbers, with Δr and Δz much smaller than L_{Rn} and L_{Pb}. The rings are enumerated by i, j, where $i = 1 \dots N_r$ and $j = 1 \dots N_z$. Elements with $i = 1$ are on-axis, while $j = 1$ at the bottom of the cylindrical domain, and $j = N_z$ at the top. Unlike the 1D case, where the source is infinitely long and one only considers points with $r > R_0$, for a finite seed in 2D one must also solve the equations for points above and below the seed, with $r < R_0$ and $|z| > \frac{1}{2}l$. As for the 1D case, the radius and z-coordinate of the i, j ring, r_i, z_j, are

defined at the center of its *rz* cross-section. For the inner-most $i = 1$ rings $r_1 = \frac{1}{2}\Delta r$. Points inside the seed, i.e., in rings with $r_i \leq R_0 - \Delta r/2$, and $|z_j| \leq \frac{1}{2}l - \frac{1}{2}\Delta z$, have zero number densities of ^{220}Rn, ^{212}Pb and ^{212}Bi.

Discretization of Equation (1-3) in 2D yields, for interior ring elements in the cylindrical domain (outside of the seed and not touching its wall or bases, and with $i > 1$):

$$\frac{n_{x,i,j}^{(p+1)} - n_{x,i,j}^{(p)}}{\Delta t} =$$

$$D_x \left(\frac{n_{x,i+1,j}^{(p+1)} + n_{x,i-1,j}^{(p+1)} - 2n_{x,i,j}^{(p+1)}}{\Delta r^2} + \frac{1}{r_i} \frac{n_{x,i+1,j}^{(p+1)} - n_{x,i-1,j}^{(p+1)}}{2\Delta r} + \frac{n_{x,i,j+1}^{(p+1)} + n_{x,i,j-1}^{(p+1)} - 2n_{x,i,j}^{(p+1)}}{\Delta z^2} \right)$$

$$- (\lambda_x + \alpha_x) n_{x,i,j}^{(p+1)} + s_{x,i,j}^{(p+1)} \quad \text{(C1)}$$

Equation (C1) holds also for ring elements on the external surfaces of the domain, with $i = N_r$, $j = 1$ or $j = N_z$, as the number densities for rings with $i = N_r + 1$, $j = 0$ or $j = N_z + 1$ are all zero. For ring elements on-axis ($i = 1$), above or below the seed, the condition is $(\partial n_x/\partial r)_{r=0} = 0$. Since the ^{224}Ra activity is confined to the seed wall, the z-component of the current density is set to zero on the seed bases, i.e., $(\partial n_x \partial z)_{z=\pm l/2} = 0$. Defining i_s as the radial index of ring elements touching the seed wall (i.e., $r_{i_s} = R_0 + \Delta r/2$), for ring elements with $|z_j| \leq l/2 - \Delta z/2$, Equation (C1) becomes, similarly to the 1D case:

$$\frac{n_{x,i_s,j}^{(p+1)} - n_{x,i_s,j}^{(p)}}{\Delta t} = \frac{D_x}{\Delta r^2} \left(\frac{1 + \Delta r/R_0}{1 + \Delta r/2R_0} \right) \left(n_{x,i_s+1,j}^{(p+1)} - n_{x,i_s,j}^{(p+1)} \right) +$$

$$\frac{D_x}{\Delta z^2} \left(n_{x,i_s,j+1}^{(p+1)} + n_{x,i_s,j-1}^{(p+1)} - 2n_{x,i_s,j}^{(p+1)} \right) - (\lambda_x + \alpha_x) n_{x,i_s,j}^{(p+1)} + s_{x,i_s,j}^{(p+1)} \quad \text{(C2)}$$

The source terms in Equation (C1) and (C2) are similar to the 1D case, with the additional requirement that $|z_j| < l/2$:

$$s_{Rn,i,j}^{p+1} = \frac{P_{des}(Rn)\left(\Gamma_{Ra}^{src}(0)/l\right)e^{-\lambda_{Ra}t_{p+1}}}{2\pi R_0 \Delta r (1 + \Delta r/2R_0)} \delta_{i,i_s} \cdot \left(\frac{1 - \text{sign}(|z_j| - l/2)}{2} \right)$$

$$\text{(C3)}$$

$$s_{Pb,i,j}^{p+1} = \frac{\left(P_{des}^{eff}(Pb) - P_{des}(Rn) \right)\left(\Gamma_{Ra}^{src}(0)/l \right)e^{-\lambda_{Ra}t_{p+1}}}{2\pi R_0 \Delta r (1 + \Delta r/2R_0)} \delta_{i,i_s}$$

$$\cdot \left(\frac{1 - \text{sign}(|z_j| - l/2)}{2} \right) + \lambda_{Rn} n_{Rn,i,j}^{p+1} \quad \text{(C4)}$$

$$s_{Bi,i,j}^{p+1} = \lambda_{Pb} n_{Pb,i,j}^{p+1} \quad \text{(C5)}$$

In order to solve Equation (C1) in matrix form we use linear indexing . The 2D elements $n_{x,i,j}^{(p)}$ and $s_{x,i,j}^{(p)}$ are rear-ranged in two column vectors $\widetilde{\mathbf{n}}_x^{(p)}$ and $\widetilde{\mathbf{s}}_x^{(p)}$ in sequential order. We define:

$$k(i,j) = (j - 1)N_r + i \quad \text{(C6)}$$

$$\widetilde{n}_{x,k}^{(p)} = n_{x,i,j}^{(p)} \quad \text{(C7)}$$

$$\widetilde{s}_{x,k}^{(p)} = s_{x,i,j}^{(p)} \quad \text{(C8)}$$

with $k = 1 \dots N_r N_z$. Noting that $n_{x,i\pm 1,j}^{(p)} = \widetilde{n}_{x,k\pm 1}^{(p)}$ and $n_{x,i,j\pm 1}^{(p)} = \widetilde{n}_{x,k\pm N_r}^{(p)}$, Equation (C1) can be rearranged as:

$$\widetilde{n}_{x,k}^{(p)} + \widetilde{s}_{x,k}^{(p+1)} \Delta t = M_{k,k-N_r}^{(x)} \widetilde{n}_{x,k-N_r}^{(p+1)} + M_{k,k-1}^{(x)} \widetilde{n}_{x,k-1}^{(p+1)}$$

$$+ M_{k,k}^{(x)} \widetilde{n}_{x,k}^{(p+1)} + M_{k,k+1}^{(x)} \widetilde{n}_{x,k+1}^{(p+1)} + M_{k,k+N_r}^{(x)} \widetilde{n}_{x,k+N_r}^{(p+1)} \quad \text{(C9)}$$

As for the 1D case, the matrix elements appearing in Equation (C9) depend on the values of i, j (and therefore k), in a manner that satisfies the boundary conditions. For compactness, we define the following intermediate quantities:

$$K_z^{(x)} = \frac{D_x \Delta t}{\Delta z^2} \quad \text{(C10)}$$

$$K_r^{(x)} = \frac{D_x \Delta t}{\Delta r^2} \quad \text{(C11)}$$

$$K_r^{(x+)} = \frac{D_x \Delta t}{\Delta r^2} \left(1 + \frac{\Delta r}{2r_i} \right) \quad \text{(C12)}$$

$$K_r^{(x-)} = \frac{D_x \Delta t}{\Delta r^2} \left(1 - \frac{\Delta r}{2r_i} \right) \quad \text{(C13)}$$

$$S_1^{(x)} = 1 + 2K_r^{(x)} + K_z^{(x)} + (\lambda_x + \alpha_x)\Delta t \quad \text{(C14)}$$

$$S_2^{(x)} = 1 + 2K_r^{(x)} + 2K_z^{(x)} + (\lambda_x + \alpha_x)\Delta t \quad \text{(C15)}$$

$$S_+^{(x)} = 1 + K_r^{(x+)} + 2K_z^{(x)} + (\lambda_x + \alpha_x)\Delta t \quad \text{(C16)}$$

Table 1 lists the expressions for the matrix elements $M_{k,l}^{(x)}$ for all possible cases for r_i and z_j. With these, one can write Equation (C9) in matrix form (with $K \equiv N_r N_z$):

$$\left(\begin{array}{c}\tilde{n}_{x,1}^{(p)}\\ \tilde{n}_{x,2}^{(p)}\\ \tilde{n}_{x,3}^{(p)}\\ \vdots\\ \tilde{n}_{x,N_r+1}^{(p)}\\ \tilde{n}_{x,N_r+2}^{(p)}\\ \vdots\\ \tilde{n}_{x,K-1}^{(p)}\\ \tilde{n}_{x,K}^{(p)}\end{array}\right) + \left(\begin{array}{c}\tilde{s}_{x,1}^{(p+1)}\\ \tilde{s}_{x,2}^{(p+1)}\\ \tilde{s}_{x,3}^{(p+1)}\\ \vdots\\ \tilde{s}_{x,N_r+1}^{(p+1)}\\ \tilde{s}_{x,N_r+2}^{(p+1)}\\ \vdots\\ \tilde{s}_{x,K-1}^{(p+1)}\\ \tilde{s}_{x,K}^{(p+1)}\end{array}\right)\Delta t = $$

$$\left(\begin{array}{ccccccccc} M_{1,1}^{(x)} & M_{1,2}^{(x)} & 0 & \cdots & M_{1,1+N_r}^{(x)} & \cdots & & & 0\\ M_{2,1}^{(x)} & M_{2,2}^{(x)} & M_{2,3}^{(x)} & 0 & \cdots & M_{2,2+N_r}^{(x)} & \cdots & & 0\\ 0 & M_{3,2}^{(x)} & M_{3,3}^{(x)} & M_{3,4}^{(x)} & 0 & \cdots & M_{3,3+N_r}^{(x)} & \cdots & 0\\ \vdots & & \ddots & \ddots & \ddots & & & \ddots & \vdots\\ M_{N_r+1,1}^{(x)} & 0 & \cdots & M_{N_r+1,N_r}^{(x)} & M_{N_r+1,N_r+1}^{(x)} & M_{N_r+1,N_r+2}^{(x)} & 0 & \cdots & 0\\ 0 & M_{N_r+2,2}^{(x)} & 0 & \cdots & M_{N_r+2,N_r+1}^{(x)} & M_{N_r+2,N_r+2}^{(x)} & M_{N_r+2,N_r+3}^{(x)} & \cdots & 0\\ \vdots & & \ddots & & & & \ddots & \ddots & \vdots\\ 0 & \cdots & 0 & M_{K-1,K-1-N_r}^{(x)} & 0 & \cdots & M_{K-1,K-2}^{(x)} & M_{K-1,K-1}^{(x)} & M_{K-1,K}^{(x)}\\ 0 & \cdots & 0 & M_{K,K-N_r}^{(x)} & 0 & \cdots & M_{K,K-1}^{(x)} & M_{K,K}^{(x)}\end{array}\right)\left(\begin{array}{c}\tilde{n}_{x,1}^{(p+1)}\\ \tilde{n}_{x,2}^{(p+1)}\\ \tilde{n}_{x,3}^{(p+1)}\\ \vdots\\ \tilde{n}_{x,N_r+1}^{(p+1)}\\ \tilde{n}_{x,N_r+2}^{(p+1)}\\ \vdots\\ \tilde{n}_{x,K-1}^{(p+1)}\\ \tilde{n}_{x,K}^{(p+1)}\end{array}\right)$$

$$(C17)$$

or, equivalently: $\tilde{\mathbf{n}}_x^{(p)} + \tilde{\mathbf{s}}_x^{(p+1)}\Delta t = \mathbf{M}_x\tilde{\mathbf{n}}_x^{(p+1)}$. As for the 1D case, multiplying on the left by the inverse of $\mathbf{M}_x$, gives: $\tilde{\mathbf{n}}_x^{(p+1)} = \mathbf{M}_x^{-1}(\tilde{\mathbf{n}}_x^{(p)} + \tilde{\mathbf{s}}_x^{(p+1)}\Delta t)$. The values of $n_{x,i,j}^{(p+1)} = \tilde{n}_{x,k}^{(p+1)}$ are then updated for all possible

TABLE 1 Matrix elements in 2D.

Case	$M_{k,k-N_r}^{(x)}$	$M_{k,k-1}^{(x)}$	$M_{k,k}^{(x)}$	$M_{k,k+1}^{(x)}$	$M_{k,k+N_r}^{(x)}$
$R_0 + \frac{\Delta r}{2} < r_i < R_{max} - \frac{\Delta r}{2}$ & $|z_j| < Z_{max} - \frac{\Delta z}{2}$	$-K_z^{(x)}$	$-K_r^{(x-)}$	$S_2^{(x)}$	$-K_r^{(x+)}$	$-K_z^{(x)}$
$\frac{\Delta r}{2} < r_i \le R_0 + \frac{\Delta r}{2}$ & $\frac{l}{2} + \frac{\Delta z}{2} < |z_j| < Z_{max} - \frac{\Delta z}{2}$	$-K_z^{(x)}$	$-K_r^{(x-)}$	$S_2^{(x)}$	$-K_r^{(x+)}$	$-K_z^{(x)}$
$r_i = R_0 + \frac{\Delta r}{2}$ & $|z_j| = \frac{l}{2} + \frac{\Delta z}{2}$	$-K_z^{(x)}$	$-K_r^{(x-)}$	$S_2^{(x)}$	$-K_r^{(x+)}$	$-K_z^{(x)}$
$r_i = R_0 + \frac{\Delta r}{2}$ & $|z_j| < \frac{l}{2}$	$-K_z^{(x)}$	0	$S_+^{(x)}$	$-K_r^{(x+)}$	$-K_z^{(x)}$
$\frac{\Delta r}{2} < r_i < R_0$ & $z_j = \frac{l}{2} + \frac{\Delta z}{2}$	0	$-K_r^{(x-)}$	$S_1^{(x)}$	$-K_r^{(x+)}$	$-K_z^{(x)}$
$\frac{\Delta r}{2} < r_i < R_0$ & $z_j = -\frac{l}{2} - \frac{\Delta z}{2}$	$-K_z^{(x)}$	$-K_r^{(x-)}$	$S_1^{(x)}$	$-K_r^{(x+)}$	0
$r_i = \frac{\Delta r}{2}$ & $\frac{l}{2} + \frac{\Delta z}{2} < |z_j| < Z_{max} - \frac{\Delta z}{2}$	$-K_z^{(x)}$	0	$S_2^{(x)}$	$-K_r^{(x+)}$	$-K_z^{(x)}$
$r_i = R_{max} - \frac{\Delta r}{2}$ & $|z_j| < Z_{max} - \frac{\Delta z}{2}$	$-K_z^{(x)}$	$-K_r^{(x-)}$	$S_2^{(x)}$	0	$-K_z^{(x)}$
$\frac{\Delta r}{2} < r_i < R_{max} - \frac{\Delta r}{2}$ & $z_j = Z_{max} - \frac{\Delta z}{2}$	$-K_z^{(x)}$	$-K_r^{(x-)}$	$S_2^{(x)}$	$-K_r^{(x+)}$	0
$\frac{\Delta r}{2} < r_i < R_{max} - \frac{\Delta r}{2}$ & $z_j = -Z_{max} + \frac{\Delta z}{2}$	0	$-K_r^{(x-)}$	$S_2^{(x)}$	$-K_r^{(x+)}$	$-K_z^{(x)}$
$r_i = \frac{\Delta r}{2}$ & $z_j = Z_{max} - \frac{\Delta z}{2}$	$-K_z^{(x)}$	0	$S_2^{(x)}$	$-K_r^{(x+)}$	0
$r_i = \frac{\Delta r}{2}$ & $z_j = -Z_{max} + \frac{\Delta z}{2}$	0	0	$S_2^{(x)}$	$-K_r^{(x+)}$	$-K_z^{(x)}$
$r_i = \frac{\Delta r}{2}$ & $z_j = \frac{l}{2} + \frac{\Delta z}{2}$	0	0	$S_2^{(x)}$	$-K_r^{(x+)}$	$-K_z^{(x)}$
$r_i = \frac{\Delta r}{2}$ & $z_j = -\frac{l}{2} - \frac{\Delta z}{2}$	$-K_z^{(x)}$	0	$S_2^{(x)}$	$-K_r^{(x+)}$	0
$r_i = R_{max} - \frac{\Delta r}{2}$ & $z_j = Z_{max} - \frac{\Delta z}{2}$	$-K_z^{(x)}$	$-K_r^{(x-)}$	$S_2^{(x)}$	0	0
$r_i = R_{max} - \frac{\Delta r}{2}$ & $z_j = -Z_{max} + \frac{\Delta z}{2}$	0	$-K_r^{(x-)}$	$S_2^{(x)}$	0	$-K_z^{(x)}$
$r_i < R_0$ & $|z_j| < \frac{l}{2}$	0	0	1	0	0

values of i, j. Once the new number densities are known in all ring elements, the alpha dose components are updated:

$$Dose_\alpha^{(p+1)}(RnPo; i, j) = Dose_\alpha^{(p)}(RnPo; i, j)$$

$$+ \frac{E_\alpha(RnPo)}{\rho} \lambda_{Rn} n_{Rn,i,j}^{(p+1)} \Delta t$$

$$(C18)$$

$$Dose_\alpha^{(p+1)}(BiPo; i, j) = Dose_\alpha^{(p)}(BiPo; i, j)$$

$$+ \frac{E_\alpha(BiPo)}{\rho} \lambda_{Bi} n_{Bi,i,j}^{(p+1)} \Delta t$$

$$(C19)$$

As for the 1D case, the time step can be modified in many ways. Here we chose to update it according to the relative change in the overall activity (sum over all isotopes in all ring elements).